An efficient method for reliability-based design optimization of structures under random excitation by mapping between reliability and operator norm

Youbao Jiang[a], Xuyang Zhang[a], Michael Beer[b,c], Hao Zhou[a], Yu Leng[a,*]

[a] *School of Civil Engineering, Changsha University of Science and Technology, Changsha 410114, China*
[b] *Institute for Risk and Reliability, Leibniz University Hannover, Callinstr. 34, Hannover 30167, Germany*
[c] *Institute for Risk and Uncertainty, University of Liverpool, Liverpool L69 7ZF, United Kingdom*

Abstract: Reliability-based design optimization (RBDO) can fulfill both reliability and economic requirements by considering the stochastic properties of structure and excitation. However, the computational efficiency of this optimization is hindered by the nested loops involved in reliability analysis and optimization processes. In order to overcome this limitation, a novel method is proposed for structures subjected to random excitation, which is based on the mapping between operator norm and reliability index. This approach necessitates effectuating the transformation of the optimization objective from reliability indexes to operator norms with a small number of samples, thereby eliminating the laborious process of nested loops. It can effectively solve design optimization problems with reliability constraints, particularly for structures with explicit structural response under random excitation. Four examples are presented to demonstrate the effectiveness and applicability of the proposed method.

Keywords: Reliability-based design optimization, Operator norm, Dynamic reliability, Random excitation, Function fitting

1. Introduction

The response of structures under natural disasters such as earthquakes, typhoons, and tsunamis is typically a stochastic dynamic process. In order to guarantee the safety of structures throughout their service life, it is essential to consider the reliability of structures under random excitation. The first excursion reliability is the most relevant performance measure for the design of engineering structures, as it effectively describe the reliability performance of structures under random excitation. However, it is also the least analytically tractable [1]. Thus, it is necessary to evaluate the safety performance of structures from a probabilistic perspective, and reliability-based design optimization (RBDO) can better ensure structural safety.

With the advancement of reliability analysis technology, the application of RBDO has expanded to various engineering fields. RBDO allows for the assessment of economic feasibility among different design alternatives while simultaneously meeting reliability specifications [2-3]. However, the direct implementation of RBDO in practical engineering designs is constrained by the nested loops involved in the optimization process. These nested loops result in high computational costs for each optimization result, which is particularly significant in dynamic reliability problems. To improve the efficiency and practicality of RBDO, several methods have been proposed [4], including the improved double-loop method [5-6], single-loop method [7-9], surrogate model method [10-12], and decoupling method [13-16].

Among these methods, the improved double-loop method aims to increase the computational efficiency of the inner loop by employing efficient reliability analysis techniques e.g. probability density evolution [17-18], importance sampling [19], and subset simulation [20]. This method assesses the failure probability of the current sample group in inner loop. Subsequently, the outer loop then identifies the optimal solution that satisfies the probability constraint based on the results of the reliability analysis. On the other hand, the single-loop method simplifies the double-loop optimization problem into a single-level problem and solves it as a standard optimization problem. In this approach, the most commonly used methods replace the lower-level optimization problems with their Karush-Kuhn-Tucker (KKT) conditions. The surrogate model method utilizes various surrogate models obtained through interpolation or fitting of training samples in reliability analysis. These surrogate models approximate implicit performance functions and corresponding limit states. Optimization based on the fitted surrogate models significantly improves efficiency, although the accuracy depends greatly on the chosen form of the surrogate model e.g. multiple response surfaces [11], Kriging surrogate models [22], and polynomial chaos expansion [23]. Lastly, the decoupling method employs mathematical transformations to decouple the inner loop and outer loop, thereby enhancing optimization efficiency. By adopting suitable decoupling strategies, the complexity of optimization problems can be greatly reduced when addressing with specific RBDO objectives[24-26].

In the case of dynamic RBDO problems involving discrete design variables

under Gaussian excitation, Feas and Valdebenito [27] utilize the operator norm as a measure of structural reliability under random excitation. They employ an operator norm framework to minimize the failure probability of linear systems influenced by random excitations. This approach can also extended to nonlinear systems through statistical linearization methods [28]. Additionally, it can be applied to fuzzy reliability evaluation in the presence of cognitive uncertainty and to assess the failure probability of structures using the operator norm under imprecise conditions [29]. Although some studies have demonstrated the potential of operator norms to achieve a fully decoupling of RBDO under specific circumstances, the existing research in this area remains relatively limited and lacks a clear association between operator norms and reliability indexes. Jerez et al. [30] summarized the reliability-based design optimization methods for structural systems under random excitation and pointed out that a heuristic framework based on operator norm optimization can effectively handle reliability optimization subject to standard constraints. The main idea is to heuristically replace the original failure probability objective function, with a function defined in terms of a matrix norm.

The motivation of this study is to expand the application of operator norms to RBDO problems. The proposed mapping method aims to satisfy both efficiency and accuracy requirements, while only analyzing a small number of samples to transform optimization objectives from reliability indexes to operator norms. This approach allows the entire optimization process to be independent of dynamic reliability analysis. The remaining sections of this contribution are organized as follows: Section 2 presents the RBDO method and its limitations. Section 3 introduces the mapping method for reliability constraints using operator norms. Section 4 utilizes four examples to demonstrate the rationality and effectiveness of the proposed method. Finally, Section 5 provides a summary of the conclusions.

2. Problem statement

The RBDO problem involves discrete design variables and probabilistic constraints, and it usually required that the response at a specific position in the structure does not exceed the safety threshold. This problem can be classified into two primary types: one aims to constrain the consumption of construction material while maximizing the reliability index, and the other aims to constrain the reliability indexes while minimizing the consumption of construction material. Mathematically, these

types can be formulated as follows:

$$\begin{aligned}&\max \beta_i\\&\text{subject to:}\\&\sum_{j=1}^{n} x_j V_j \le V^{\text{th}}\\&x_j \in \mathrm{N}\\&V_j \in V^{\text{data}}\end{aligned} \tag{1}$$

$$\begin{aligned}&\min \sum_{j=1}^{n} x_j V_j;\\&\text{subject to}\\&\beta_i \ge \beta_i^{\text{th}}\\&x_j \in \mathrm{N}\\&V_j \in V^{\text{data}}\end{aligned} \tag{2}$$

where x_j and V_j correspond to the number and material volume of discrete design variables, respectively; β_i represents the reliability index of the structure, i=1,2,...,n_R; n_R depends on the response parts of interest. The reliability index β_i can be calculated by:

$$\beta_i = \Phi^{-1}(1 - P_{fi}), i = 1, 2, ..., n_R \tag{3}$$

The failure criterion for the structure is determined by whether its response under Gaussian load excitation exceeds the safety limit b_i, which is assessed through the first excursion probability [31]. The failure probability P_f can be expressed as:

$$P_{fi} = P(\bigcup_{k=1}^{n_T} \{\exists t \in [0, T] : | u_{ik}(t) | > b_{ik}\}), i = 1, 2, ..., n_R \tag{4}$$

where n_T is the total number of time instants considered. The failure probability of the structure can be computed using the Monte Carlo sampling method, which is determined by:

$$P_{fi} = \frac{1}{N} \sum_{l=1}^{N} I_i[Y_l(t)], i = 1, 2, ..., n_R \tag{5}$$

$$I_i[Y_l(t)] = \begin{cases} 1, |u_{il}(t)| \ge b_i \\ 0, |u_{il}(t)| < b_i \end{cases}, i = 1, 2, ..., n_R \tag{6}$$

Among these equations, $u(t)$ represents the dynamic response of the structure at any given time, which can be calculated by:

$$u_i(t) = \sum_{k=1}^{n_T} h_i\left(t_k - t_{\mathrm{m}}\right) f(t)\Delta t, i = 1, 2, ..., n_R \tag{7}$$

where $h_i\left(t_k - t_{\mathrm{m}}\right)$ represents the structural response induced by a pulse load at any given time.

This current RBDO procedure entails the computation of the reliability index for every design sample, followed by the utilization of algorithms to search for the optimal solution. However, the extensive sampling required in Eq.(5) and Eq.(6) results in a time-consuming analysis of the reliability for each sample group.

To address this challenge, we propose a novel method based on a mapping transformation. This method converts the optimization objective from the reliability index to the operator norm, thereby eliminating the need for the laborious reliability analysis procedure. By employing the operator norm as a surrogate, which is comparatively easier to calculate, the RBDO process can be carried out more efficiently.

3. Mapping between operator norm and reliability index in RBDO

3.1 Operator norm of structural dynamic response

The operator norm can be used to measure the size of certain linear operators, for a matrix **A** of dimensions $m \times n$ and a vector v of dimensions $n \times 1$, the theory of operator norm can be summarized as follows: the operator **A** never amplifies the length of any vector v by more than a certain factor c. In other words, there exists a lower bound c such that the aforementioned inequality holds true for all vectors v. This concept can be expressed as:

$$\| \mathbf{A} \|_{p^{(1)}, p^{(2)}} = \inf \left\{ c \geq 0 : \| \mathbf{A}v \|_{p^{(1)}} \leq c \| v \|_{p^{(2)}} \right\} \tag{8}$$

where $\inf\{\cdot\}$ denotes the infimum value and $\|\cdot\|_{p(1),p(2)}$ denotes the operation rules for the operator norm, which can be found in Table 1.

Table 1 Operation rules for the operator norm[29]

Operation rules		$p^{(1)}$		
		l_1	l_2	l_∞
$p^{(2)}$	l_1	Maximum l_1 norm of column	Maximum l_2 norm of column	Maximum l_∞ norm of column
	l_2	NP-hard	Maximum singular value	Maximum l_2 norm of row
	l_∞	NP-hard	NP-hard	Maximum l_1 norm of row

In the case of the first excursion failure mechanism, the structural failure depends on whether the maximum value of the dynamic response process surpasses the safety threshold. In order to ensure that the operator norm value of the structural response remains unaffected by randomness, the process can be formulated as a linear superposition of a series of orthogonal functions and products of random variables, employing the Karhunen-Loève (K-L) expansion within the operator norm framework [32]. If the Gaussian random excitation is denoted by $f(t,\xi)$, the random process can be expanded as:

$$f(t) = \overline{f}(t) + \phi_n(t)\sqrt{\lambda_n}\xi_n \tag{9}$$

In this context, f (t) represents an n_T×1 random load vector, whereas $\overline{f}(t)$ represents the average value of the random process. φ_n and λ_n represent the eigenvectors and eigenvalues of the auto-covariance matrix of the random process with dimensions of n_T×n_{KL} and n_{KL}×n_{KL} matrices, respectively. The vector ξ_n represents the realization of standard Gaussian random variables, which is a n_{KL}×1 vector. For a discrete Gaussian process with a mean of zero, that is $\overline{f}(t) = 0$, the random process can be represented as:

$$f(\xi) = \phi\sqrt{\lambda}\xi \tag{10}$$

Based on the established definition of first excursion reliability, it is desirable for the absolute values of the responses of interest to remain below the predetermined threshold levels. As a result, the normalized response function within the operator norm framework is defined as follows:

$$r(y,\xi) = \| A(y)\xi \|_\infty \tag{11}$$

Here, y represents the discrete design variables of the structure. $A(y)$ is a ($n_R n_T$)×n_{KL} matrix, where the matrix elements correspond to the operator norm values of the structural response. By setting $p^{(1)}\to\infty$ and $p^{(2)}$=2 in Eq.(8), the following relationship can be established through the operator norm theorem and the calculation of the normalized response function [15].

$$\| A(y) \|_{\infty,2} = \inf\left\{ c(y) \ge 0 : \| A(y)\xi \|_\infty \le c(y) \| \xi \|_2 \right\} \tag{12}$$

In the scenario involving multiple degrees of freedom, $\boldsymbol{A_i}(\boldsymbol{y})$ is a matrix that collects all matrices associated with the calculation of the i-th response, normalized by threshold levels, which is defined as:

$$\boldsymbol{A}_i(\boldsymbol{y}) = b_i^{-1}\begin{bmatrix} \boldsymbol{a}_{i1}(\boldsymbol{y}) \\ \boldsymbol{a}_{i2}(\boldsymbol{y}) \\ \vdots \\ \boldsymbol{a}_{in_T}(\boldsymbol{y}) \end{bmatrix}, i = 1,...,n_R \tag{13}$$

where b_i represents the security boundaries corresponding to different cases. According to Table 1, the solution for the matrix $\|\mathrm{A}(y)\|_{\infty,2}$ is equivalent to the maximum row of matrix **A(*y*)**, which can be expressed as:

$$\| \boldsymbol{A}(\boldsymbol{y}) \|_{\infty,2} = \max_{\substack{i=1,\ldots,n_R \\ k=1,\ldots,n_T}} \left(\sqrt{\boldsymbol{a}_{\mathrm{ik}} \boldsymbol{a}_{\mathrm{ik}}^T} \right) \tag{14}$$

where a_{ik} represents the row of matrix **A**, which is calculated based on the response at any discrete time.

The dynamic response of the structure under random excitation can be calculated using the motion equations of the structure, as described in:

$$\boldsymbol{M}(\boldsymbol{y})\ddot{\boldsymbol{x}}(t,\boldsymbol{y},\xi) + \boldsymbol{C}(\boldsymbol{y})\dot{\boldsymbol{x}}(t,\boldsymbol{y},\xi) + \boldsymbol{K}(\boldsymbol{y})\boldsymbol{x}(t,\boldsymbol{y},\xi) = \rho f(t,\xi) \tag{15}$$

where **M**, **C** and **K** are matrices representing the mass, damping, and stiffness of the system, respectively, with dimensions of $n_D \times n_D$. Here, n_D represents the number of freedom degrees. The vector y encompasses the discrete design variables that influence the mass, damping, and stiffness matrices, and t denotes time. Furthermore, ρ is a $n_D \times 1$ vector corresponding to the coupling load $f(t,\xi)$, while $\ddot{\boldsymbol{x}}(t,\boldsymbol{y},\xi)$, $\dot{\boldsymbol{x}}(t,\boldsymbol{y},\xi)$ and $\boldsymbol{x}(t,\boldsymbol{y},\xi)$ represent the acceleration, velocity, and displacement, respectively, each with dimensions of $n_D \times 1$.

Based on the Duhamel's integral method, the response of the structure is obtained by summing up the dynamic responses caused by all discrete impulse loads occurring before the given time. The structural response can be expressed as shown in:

$$u_i(t) = \int_0^{\mathrm{t}} f(\tau) h_i(t-\tau) d\tau, i = 1,...,n_R \tag{16}$$

where $h_i(t-\tau)$ represents the unit impulse response function. If the structural displacement vector x is adopted as the response of interest, the impulse response can be expressed as:

$$h_i(t,y) = \sum_{v=1}^{n_D} \frac{\alpha_{i,v} e^{-\zeta_{\mathrm{n}}(y)\omega_{\mathrm{n}}(y)t}}{\omega_d(y)} \sin\left(\omega_d(y)t\right), i = 1,...,n_R \tag{17}$$

where ζ_n represents the structural damping ratio; ω_n and ω_d represent the natural frequency and damping frequency, with the relationship $\omega_d = \omega_{\mathrm{n}}\sqrt{(1-\zeta_n^2)}$. In

addition, $\alpha_{i,v}$ are the model participation factor matrix, which is defined as:

$$\alpha_{i,v}=\frac{q_i^T\phi_v(y)\phi_v(y)^T\rho}{\phi_v(y)^T M(y)\phi_v(y)}, i=1,...,n_R, v=1,...,n_D \tag{18}$$

where $\phi_v(y)$ represents the eigenvectors associated with the eigenproblem of the undamped equation of motion, and q_i is a vector such that $u_i=q_i^T x$.

By discretizing the time units and expanding the random excitation through Eq.(10), Eq.(16) can be transformed into:

$$\begin{aligned} u_i(t_k,y,\xi)&=\sum_{m=1}^{k}\epsilon_{\mathrm{m}}h_i(y,t_k-t_{\mathrm{m}})\,f(t_{\mathrm{m}},\xi)\Delta t=\sum_{m=1}^{k}\epsilon_{\mathrm{m}}h_i(y,t_k-t_{\mathrm{m}})\left(\sum_{\mathrm{n}=1}^{n_{KL}}\phi_{\mathrm{m,n}}\sqrt{\lambda_{\mathrm{n}}}\xi_{\mathrm{n}}\right)\Delta t \\ &=a_{ik}(y)\xi, i=1,\ldots,n_{\mathrm{R}}, k=1,\ldots,n_{\mathrm{T}} \end{aligned} \tag{19}$$

where $\phi_{m,n}$ represents the element at the position of the matrix $\phi(m,n)$, and ϵ_{m} takes the value of 0.5 when m=1 or k, otherwise it is set to 1. $h_i(y,t_k-t_{\mathrm{m}})$ signifies the response induced by the impulse load at any given time.

By eliminating the standard Gaussian random vector, the expression of the row vector a_k of the operator norm matrix can be obtained. In this case, the largest row of matrix A(y) corresponds to the operator norm of the structural response, as illustrated in:

$$\begin{aligned} a_{ik}(y)&=b_i^{-1}[\sum_{m=1}^{k}\Delta t\epsilon_{\mathrm{m}}h_i(y,t_k-t_{\mathrm{m}})\psi_{m,1}\sqrt{\lambda_1},...,\sum_{m=1}^{k}\Delta t\epsilon_{\mathrm{m}}h_i(y,t_k-t_{\mathrm{m}})\psi_{m,n_{KL}}\sqrt{\lambda_{n_{KL}}}], \\ &i=1,\ldots,n_{\mathrm{R}}, k=1,\ldots,n_{\mathrm{T}} \end{aligned} \tag{20}$$

Significantly, the calculation of the operator norm does not necessitate a substantial number of samples, as it can be obtained through a single time integration calculation. Furthermore, the operator norm value remains unaffected by the standard Gaussian random vector ξ_n, and this characteristic makes the calculation of the structural response operator norm very efficient. Therefore, a mapping between the operator norm and reliability performance can be established, with the operator norm serving as a more computable surrogate, leading to improved efficiency in RBDO.

3.2 Mapping function for constraint transformation in RBDO

Based on the aforementioned approaches, the operator norm $\|A(y)\|_{\infty,2}$ and dynamic reliability index β of the structural response can be calculated. In order to establish the mapping relationship between β and $\|A(y)\|_{\infty,2}$, a function φ is constructed

through Eq.(21). Conventionally, various functions can be chosen for φ, such as polynomial functions, exponential functions, logarithmic functions, trigonometric functions, etc. Herein, the polynomial function is selected as the fitting function. By employing least squares fitting, the mapping function can be obtained with limited sample points, as shown in:

$$|| \boldsymbol{A}(\boldsymbol{y}) ||_{\infty,2} = \varphi(\beta) = \alpha_0 + \alpha_1\beta + \alpha_2\beta^2 ... + \alpha_n\beta^n \tag{21}$$

where n is the degree of polynomial fitting function. It is recommended to use an initial polynomial fitting function with a degree of n=3, and the degree of function can be adjusted to achieve accurate results.

$$\min_{\varphi} \sum_{i=1}^{m-1} \delta_i^2 = \sum_{i=1}^{m-1} \left(\varphi\left(\beta_i^{train}\right) - || A_i(y) ||_{\infty,2}^{train} \right)^2 \tag{22}$$

where m is the number of samples in the data set. In order to ensure the high accuracy of the fitted mapping function, a leave-one-out cross validation is used for error checking. If the fitting function effectively predicts the test samples and satisfies Eq.(23) as well, it can be considered as the output for the mapping function. It is recommended to set ε as 0.001. If the fitted mapping function fails to meet the accuracy requirements, the degree of the mapping function can be increased and the fitting process repeated.

$$\left(\varphi\left(\beta_i^{\text{test}}\right) - || A_i(y) ||_{\infty,2}^{\text{test}} \right)^2 \le \varepsilon \tag{23}$$

Based on this mapping function, the constraint can be reformulated, and the original optimization problem can be transformed into:

$$\begin{aligned} &\min || \boldsymbol{A}(\boldsymbol{y}) ||_{\infty,2} \\ &\text{subject to:} \\ &\sum_{i=1}^{n} x_i V_i \le V^{\text{th}} \\ &x_i \in \text{N} \\ &V_i \in V^{\text{data}} \end{aligned} \tag{24}$$

$$\begin{aligned} &\min \sum_{i=1}^{n} x_i V_i; \\ &\text{subject to:} \\ &|| \boldsymbol{A}(\boldsymbol{y}) ||_{\infty,2} \le || \boldsymbol{A}(\boldsymbol{y}) ||_{\infty,2}^{th} \\ &x_i \in \text{N} \\ &V_i \in V^{\text{data}} \end{aligned} \tag{25}$$

By utilizing the operator norm inequality to eliminate Gaussian random vectors,

the safety of the structure can be assessed using the operator norm. The operator norm $\|A(y)\|_{\infty,2}$ is a dimensionless constant that is inversely proportional to the reliability index β. Therefore, a mapping relationship between $\|A(y)\|_{\infty,2}$ and β can be established. This transformation simplifies the extensive sampling analysis into a single calculation of the dynamic response operator norm, significantly reducing computational efforts. Upon verification, it has been determined that the computational efficiency can be improved by over 100 times when faced with high-capacity optimization problems.

3.3 Flowchart of RBDO based on mapping

By transforming the optimization objective into the operator norm, RBDO can bypass the cumbersome process of reliability analysis, and significantly enhance optimization efficiency. The proposed method for RBDO under random excitation is shown in Fig. 1, a solution procedure is given as follows:

(1) Establish RBDO problem formulations based on discrete variables and probability constraints.

(2) Randomly select m sample groups as the data set from the discrete design variables. It is recommended to take 1/500 of the total number of optimized samples and not less than 50.

(3)Calculate the operator norm and reliability index of the data set through Eq.(3) and (20).

(4) Take one sample in the dataset as the test set, and use the remaining samples as the training set for function fitting according to Eq.(21) and (22). Repeat the above process m times to ensure that each sample is used as a test set.

(5) Substitute each test set sample into the corresponding mapping function and use Eq.(23) to measure the error. If there is a mapping function φ that meets the error requirements, output the one with the smallest fitting error. Otherwise, let n=n+1 and return to Step 3.

(6) Transform the reliability index constraint into a deterministic constraint in the initial RBDO problem by mapping function φ. Use the transformed operator norm as the objective for optimization. Output the desired optimization results based on the optimization objective.

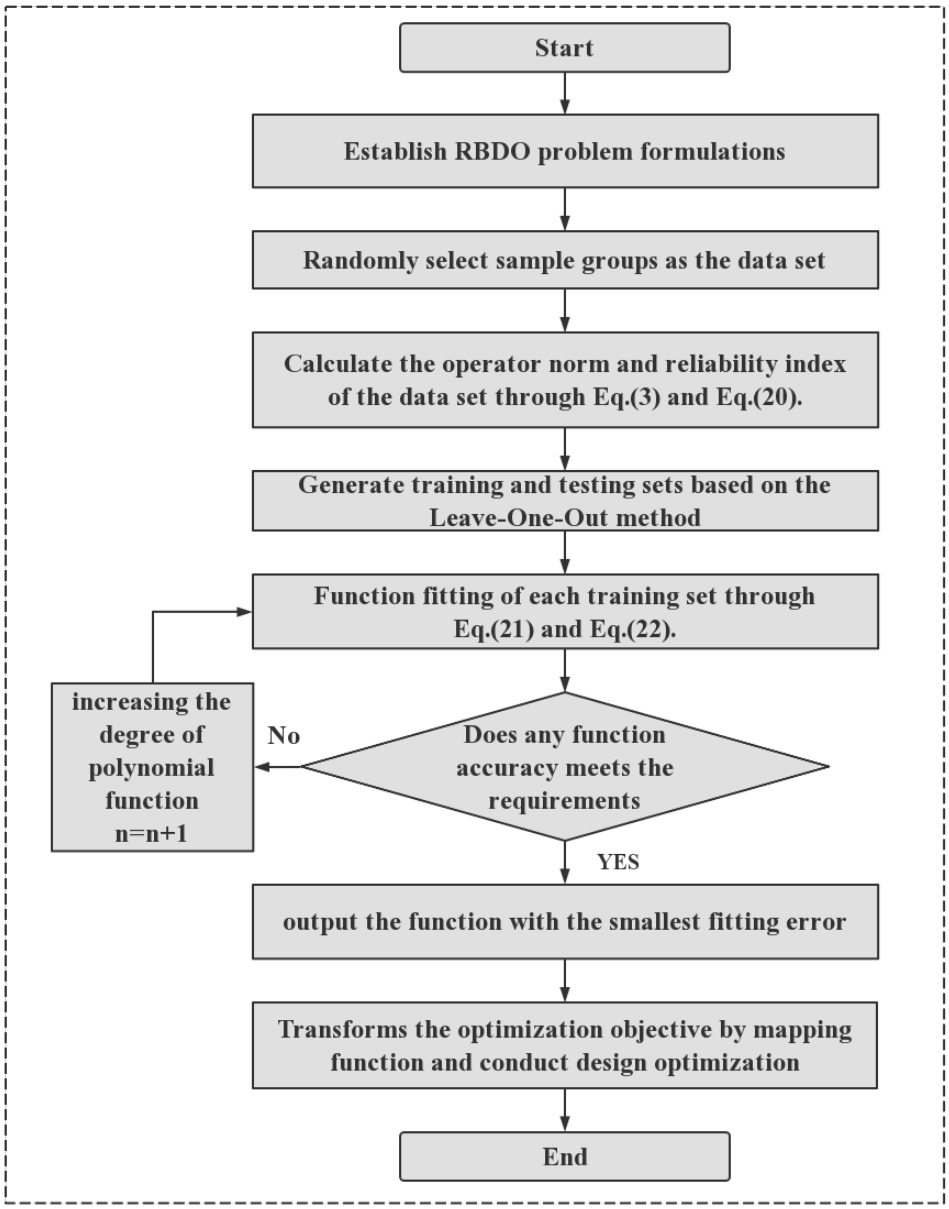

Fig. 1 Flowchart of RBDO based on the proposed method

4. Examples

4.1 Example 1: Optimization of mass and stiffness for single-degree-of-freedom oscillators

The first example focuses on a single-degree-of-freedom oscillator subjected to discrete Gaussian white noise excitation. The Gaussian white noise has a mean of zero, a spectral density of S_0=5×10^{-4}m^2/s^3, a duration of T=10s, and a discretization time unit of Δt=0.01s. The mass of the oscillator and the stiffness of the spring are discrete design variables, with values of m={2.50, 2.51, 2.52, ..., 2.99, 3.00}×10^{4}kg and

k={4.50, 4.51, 4.52, ..., 4.99, 5.00}×10^6N/m. The damping ratio is ζ=3%. It is assumed that failure occurs when the displacement of the oscillator exceeds 5mm. Two types of reliability design optimization problems are conducted, considering a total of m=2000 sample groups.

Optimization Case 1: The objective is to determine the maximum mass for the oscillator with the reliability index not less than 2.40.

Optimization Case 2: The objective is to determine the minimum stiffness for the oscillator with the reliability index not less than 2.40.

The two reliability optimization problems are described as follows:

$$\begin{aligned} &\max m \\ &\text{subject to:} \\ &\beta \geq 2.40 \\ &k \in 10^6 \times \{4.50, 4.51, 4.52, \ldots 4.99, 5.00\}\text{N/m} \\ &m \in 10^4 \times \{2.50, 2.51, 2.52, \ldots, 2.99, 3.00\}\text{kg} \end{aligned} \tag{26a}$$

$$\begin{aligned} &\min k \\ &\text{subject to:} \\ &\beta \geq 2.40 \\ &k \in 10^6 \times \{4.50, 4.51, 4.52, \ldots 4.99, 5.00\}\text{N/m} \\ &m \in 10^4 \times \{2.50, 2.51, 2.52, \ldots, 2.99, 3.00\}\text{kg} \end{aligned} \tag{26b}$$

The reliability index of each sample point is calculated through 1 million Monte Carlo sampling cycles, and the operator norm of the structural response can be calculated according to Eq.(5). The distribution of operator norms and reliability indexes in 50 sample groups is shown in Fig. 2, and the fitting for operator norm and reliability index of these sample points is shown in Fig. 3.

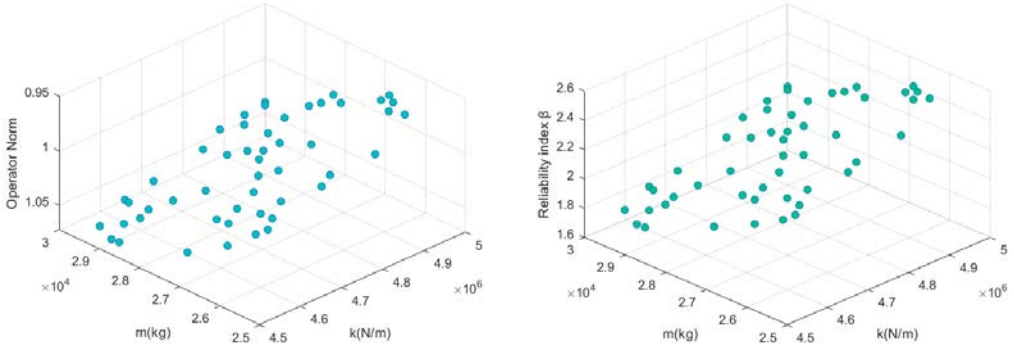

(a)Operator norm (b)Reliability index

Fig. 2 Distribution of operator norms and reliability indexes

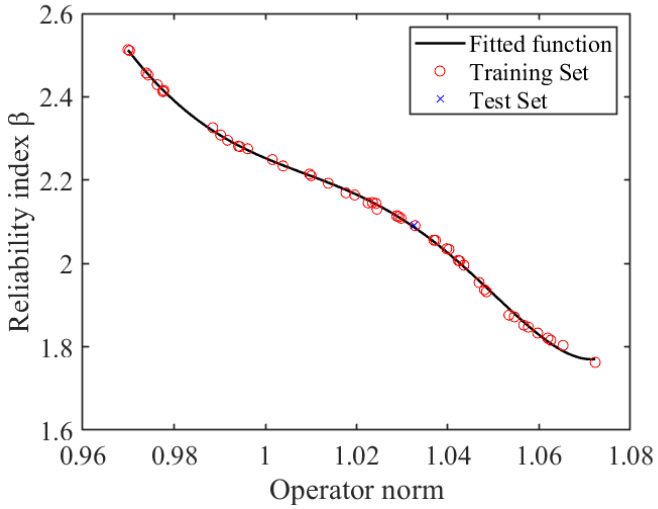

Fig. 3 The fitting situation of the mapping function

The order of the fitting function meets the accuracy requirement after reaching six, and the function is shown as follows:

$$\varphi(\beta) = -12.08\beta^6 + 151.49\beta^5 - 787.27\beta^4 + 2170.00\beta^3 - 3345.60\beta^2 + 2735.50\beta - 925.48 \tag{27}$$

The original reliability optimization problem is transformed into a deterministic optimization problem with Eq(24). The transformed optimization problem can be expressed as follows:

$$\begin{aligned} &\max m \\ &\text{subject to:} \\ &\| \boldsymbol{A}(\boldsymbol{y}) \|_{\infty,2} \le \varphi(2.40) \\ &k \in 10^6 \times \{4.50, 4.51, 4.52, \ldots 4.99, 5.00\}\text{N/m} \\ &m \in 10^4 \times \{2.50, 2.51, 2.52, \ldots, 2.99, 3.00\}\text{kg} \end{aligned} \tag{28a}$$

$$\begin{aligned} &\min k \\ &\text{subject to:} \\ &\| \boldsymbol{A}(\boldsymbol{y}) \|_{\infty,2} \le \varphi(2.40) \\ &k \in 10^6 \times \{4.50, 4.51, 4.52, \ldots 4.99, 5.00\}\text{N/m} \\ &m \in 10^4 \times \{2.50, 2.51, 2.52, \ldots, 2.99, 3.00\}\text{kg} \end{aligned} \tag{28b}$$

Based on the transformed constraint objectives, an optimization analysis was conducted on this example, and the results were compared with alternative methodologies in terms of efficiency and accuracy. The optimization results are shown in Table 2, and all computations were performed on a desktop computer with

32 GB of RAM and 12th Gen Intel(R) Core(TM) i7-12700 CPU @ 2.10 GHz.

Table 2 Optimization results for Example 1

Method	Case 1	Efficiency		Case 2	Efficiency	
		Time/h	Ratio		Time/h	Ratio
Proposed method	$m = 2.69\times10^4$ kg $k = 5.00\times10^6$ N/m β=2.40	0.16	1.0	$m = 2.50\times10^4$ kg $k = 4.65\times10^6$ N/m β=2.41	0.16	1.0
AK-MCS [33]	$m = 2.70\times10^4$ kg $k = 5.00\times10^6$ N/m β=2.39	0.55	3.4	$m = 2.50\times10^4$ kg $k = 4.62\times10^6$ N/m β=2.36	0.54	3.4
Response surface [34]	$m = 2.72\times10^4$ kg $k = 5.00\times10^6$ N/m β=2.36	0.57	3.6	$m = 2.50\times10^4$ kg $k = 4.58\times10^6$ N/m β=2.36	0.57	3.6
Monte Carlo	$m = 2.69\times10^4$ kg $k = 5.00\times10^6$ N/m β=2.40	5.26	32.9	$m = 2.50\times10^4$ kg $k = 4.65\times10^6$ N/m β=2.41	5.28	33.0

It is evident that the proposed method presents notable advantages in terms of efficiency in comparison to existing reliability design optimization methods. When compared to the direct Monte Carlo method, the proposed method demonstrates a significantly higher efficiency, approximately 33 times greater. In comparison to the AK-MCS method and the response surface method, the efficiency is still approximately 3.5 times higher. It was determined that the maximum attainable mass was 2.69×10^4 kg, and the minimum attainable stiffness was 4.65×10^6 N/m while meeting the requirement of a reliability index no less than 2.4.

4.2 Example 2: Optimization of stiffness for a three-degree-of-freedom spring damping vibration system

The second example focuses on a three-degree-of-freedom spring damping vibration system, as illustrated in Fig. 4. The system experiences identical excitation parameters as Example 1. The masses of the objects, from left to right, are known to be $m_1=5\times10^4$kg, $m_2=12\times10^4$kg, and $m_3=25\times10^4$kg. The stiffness of the springs is considered as discrete design variables, with values of k_i={2.00, 2.10, 2.20, ..., 3.90, 4.00}$\times10^6$N/m for i=1,2,3,4. The damping ratio is $c_1=c_2=c_3=c_4=0.03$. Each research object's response is treated as an independent case, and failure occurs if the

displacement exceeds 5mm. The reliability indexes corresponding to the three mass objects are β_1, β_2 and β_3.

The optimization problem aims to minimize the sum of the stiffness coefficients of the four springs while ensuring that the reliability index of each case is not less than 2.40. Considering a total of m=5000 sample groups, the reliability index for each case in this optimized scenario is calculated. The reliability optimization problem can be expressed as:

$$\begin{aligned} &\min \sum_{i=1}^{4} k_i \\ &\text{subject to:} \\ &k_i \in \{2.00, 2.10, 2.20, \cdots\ldots, 3.90, 4.00\} \times 10^6 \text{ N/m} \\ &\forall \beta_i \geq 2.40, i = 1, 2, 3. \end{aligned} \tag{29}$$

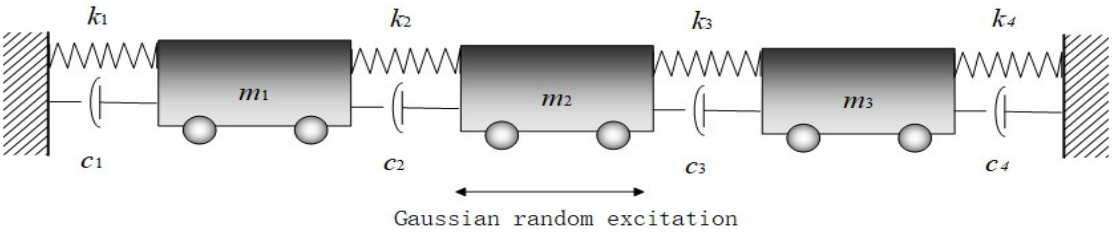

Fig. 4 Schematic diagram of a three-degree-of-freedom series spring system

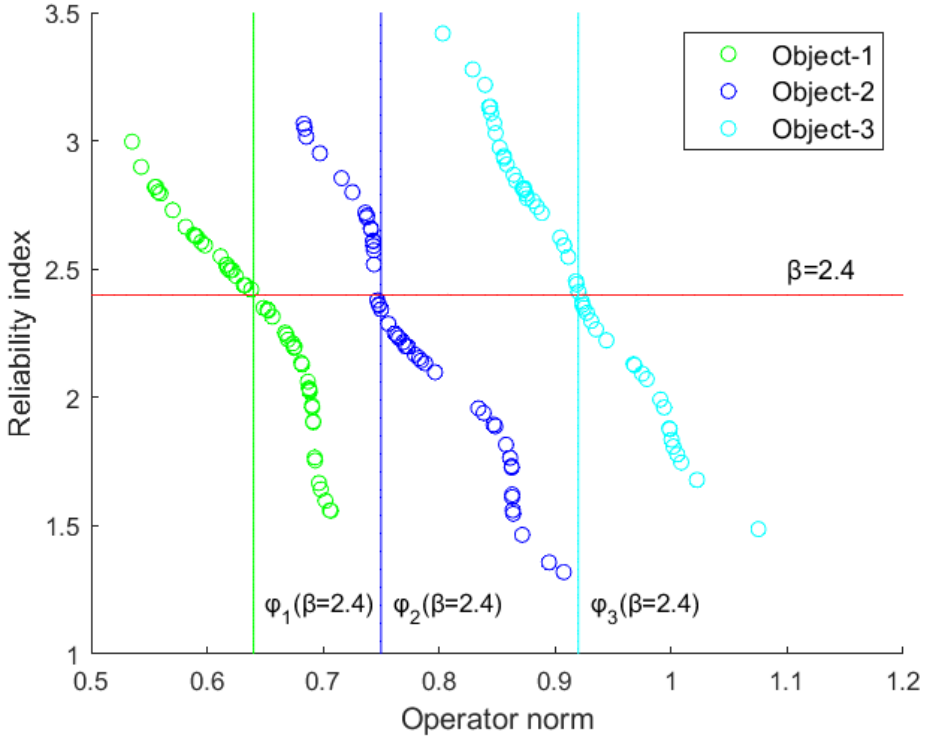

Fig. 5 Operator norm-reliability index mapping function for Example 2

In Fig. 5, a total of 50 sample points are considered for three separate failure cases. The reliability index of each sample point is calculated by 1 million Monte Carlo sampling cycles. A mapping function is then established to relate the operator norm-reliability index for the three objects, as shown below:

$$\varphi_1(\beta) = -0.12\beta^6 + 1.54\beta^5 - 7.72\beta^4 + 19.42\beta^3 - 25.32\beta^2 + 15.48\beta - 2.29 \tag{30}$$

$$\varphi_2(\beta) = 0.77\beta^6 - 10.45\beta^5 + 58.27\beta^4 - 170.13\beta^3 + 274.00\beta^2 - 230.76\beta + 80.29 \tag{31}$$

$$\varphi_3(\beta) = 0.04\beta^4 - 0.35\beta^3 + 1.27\beta^2 - 2.15\beta + 2.44 \tag{32}$$

This mapping facilitates the transformation of the optimization objective from the reliability index to the operator norm. The initial optimization problem is transformed into:

$$\begin{aligned} &\min \sum_{i=1}^{4} k_i \\ &\text{subject to:} \\ &k_i \in \{2.00, 2.10, 2.20, \cdots\ldots, 3.90, 4.00\} \times 10^6 \text{ N/m} \\ &\forall \, \| \boldsymbol{A}_j(\boldsymbol{y}) \|_{\infty,2} \le \varphi_j(2.40),\ j = 1, 2, 3. \end{aligned} \tag{33}$$

Based on the transformed optimization problem, a total of 5000 sample groups were optimized and analyzed. The obtained results are presented in Table 3. It is evident that the proposed method achieves a higher level of efficiency while also ensuring accurate calculations.

Table 3 Optimization results for Example 2

Optimization parameters		Proposed method	AK-MCS	Response surface	Monte Carlo
Stiffness	k_1 ($\times 10^6$N/m)	2.90	3.60	2.30	2.40
	k_2 ($\times 10^6$N/m)	3.10	2.50	3.40	3.30
	k_3 ($\times 10^6$N/m)	3.20	3.20	3.40	3.40
	k_4 ($\times 10^6$N/m)	3.30	3.20	3.50	3.40
	$\sum k_i$ ($\times 10^6$N/m)	12.50	12.50	12.60	12.50
Reliability index(operator norm)	$\beta_1(\|A_1(y)\|_{\infty,2})$	2.43 (0.6273)	2.41	2.44	2.42
	$\beta_2(\|A_2(y)\|_{\infty,2})$	2.40 (0.7454)	2.44	2.43	2.46
	$\beta_3(\|A_3(y)\|_{\infty,2})$	2.53 (0.9168)	2.41	2.46	2.42
Efficiency	Time/h	0.55	1.83	1.96	17.30
	Ratio	1.0	3.32	3.56	31.5

4.3 Example 3: Cost design optimization of six-story steel frame structure

The third example focuses on a six-story planar steel frame structure, as illustrated in Fig. 6. Each floor of the structure has a mass of m=5×10^{4}kg, with a floor height of h=3 meters. The beam stiffness is assumed to be infinite. The columns on each floor are selected from HM steel sections whit specific specifications. The moment of inertia I_x and section area A of the HM steel sections are considered as discrete design variables, which can be obtained from Appendix 1. The elastic modulus of the steel is E=210GPa. Considering a damping ratio of ζ=5% for all modes, failure occurs if the top displacement of the structure exceeds 0.5m under Clough-Penzien filtered possesses.

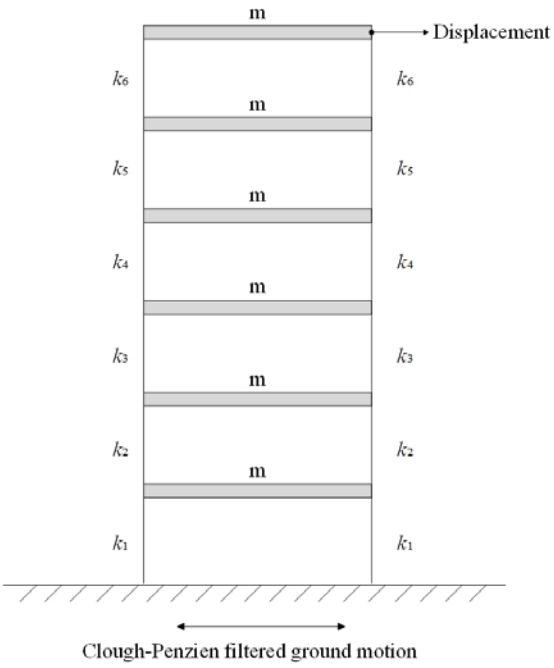

Fig. 6 Six-story steel frame structure under Clough-Penzien model excitation

The excitation experienced by the structure is modeled using the Clough-Penzien non-stationary earthquake power spectrum model [35]. The power spectral density function of the excitation is expressed as:

$$S_{\ddot{x}}(\omega)=\frac{\omega_g^4+4\xi_g^2\omega_g^2\omega^2}{(\omega_g^2-\omega^2)^2+4\xi_g^2\omega_g^2\omega^2}\frac{\omega^4}{(\omega_f^2-\omega^2)^2+4\xi_f^2\omega_f^2\omega^2}S_0 \tag{34}$$

In this equation, S_0 represents the spectral density, which is a constant that is associated with the intensity of ground motion. The parameters ω_g and ξ_g represent the characteristic frequency and damping ratio of the soil layer at the site, respectively. The parameters ξ_f and ω_f are used to filter out the low-frequency portion of the

earthquake motion. Generally, ξ_g=ξ_f and ω_f=0.1-0.2ω_g. The known parameter values are: ω_g=17.95Hz, ξ_g=0.72, ω_f=0.0856Hz, ξ_f=0.72, and S_0=50.045×10^{-4}m^2/s^3 under medium seismic conditions.

The total duration of the excitation is 15s, and the time step for discretization is Δt=0.01s. The non-stationary process is modulated by a three-stage function [36], as shown in:

$$f(t)=\begin{cases} t^2/16, 0\le t\le 4 \\ 1, 4\le t\le 10 \\ e^{-0.35(t-10)}, 10\le t\le 15 \end{cases} \tag{35}$$

The optimization problem is focused on designing the structure using a total of 20,000 sample groups, with the objective of ensuring that the reliability indexes are not less than 3.20, while simultaneously minimizing the steel usage. Assuming that the cross-sectional area of the steel on the i-th floor is represented as A_i, the optimization objectives are transformed through Eq(34), and the optimization problem is expressed as:

$$\begin{aligned} &\min \sum_{i}^{6} 2hA_i \\ &\text{subject to:} \\ &\beta_j \ge 3.20 \Rightarrow \| \boldsymbol{A}_j(\boldsymbol{y}) \|_{\infty,2} \le \varphi_j(3.20),\ j=1,2,3,4,5,6 \\ &k_i \in \mathrm{EI}_x(\mathrm{HM})\mathrm{N/m} \end{aligned} \tag{36}$$

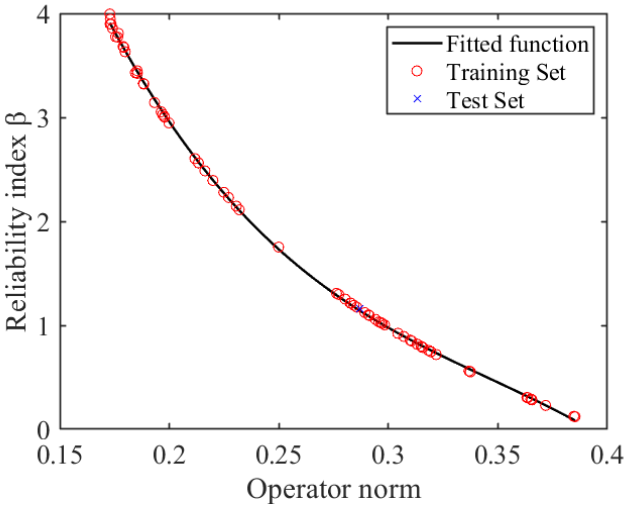

Fig. 7 Operator norm-reliability index mapping function for Example 3

$$\varphi(\beta)=-0.0023\beta^3+0.0258\beta^2-0.1236\beta+0.3986 \tag{37}$$

Fig. 7 shows the mapping function for Example 3, with a total of 50 sample points. This transformed operator norm is employed as a constraint condition within the optimization algorithm, facilitating to the design and optimization of 20,000 sample groups.

In Fig. 8, the response operator norm for these 20,000 sample groups was calculated and illustrated. The the red points on the left side correspond to valid samples with a reliability index greater than 3.2, and the blue points on the right side represent invalid samples with a reliability index lower than 3.2.Among them, the optimal design scheme is represented by a pink solid hexagon.

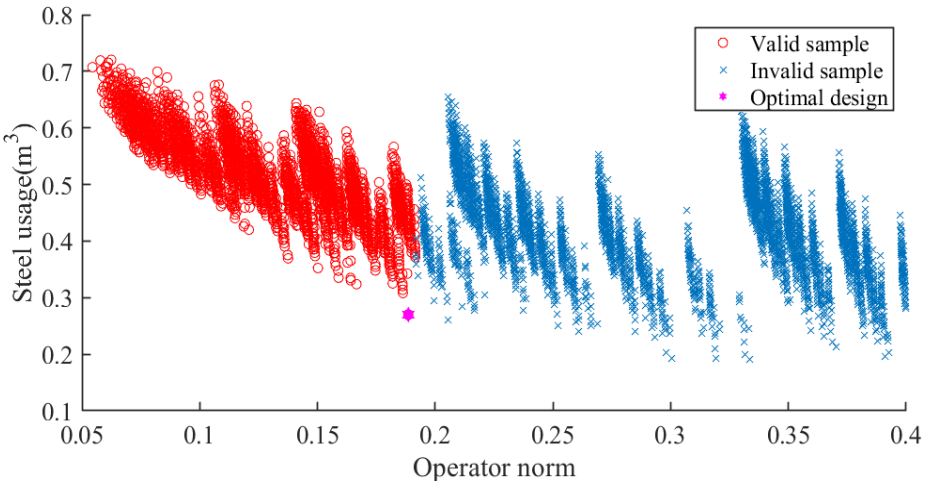

Fig. 8 Scatter plot of operator norm-steel usage

Table 4 Optimization results for Example 3

Optimization parameters		Proposed method	AK-MCS	Response surface	Monte Carlo
Steel specification	6^{th} floor	HM244×175 ×7×11	HM244×175 ×7×11	HM244×175 ×7×11	HM244×175 ×7×11
	5^{th} floor	HM294×200 ×8×12	HM244×175 ×7×11	HM294×200 ×8×12	HM294×200 ×8×12
	4^{th} floor	HM294×200 ×8×12	HM294×200 ×8×12	HM294×200 ×8×12	HM294×200 ×8×12
	3^{rd} floor	HM294×200 ×8×12	HM294×200 ×8×12	HM340×250 ×9×14	HM294×200 ×8×12
	2^{nd} floor	HM294×200 ×8×12	HM340×250 ×9×14	HM340×250 ×9×14	HM294×200 ×8×12
	1^{st} floor	HM340×250 ×9×14	HM482×300 ×11×15	HM340×250 ×9×14	HM340×250 ×9×14
β ($\|A(y)\|_{\infty,2}$)		3.21 (0.1886)	3.27	3.26	3.21
Steel usage（m^3）		26.99×10^{-2}	30.39×10^{-2}	32.50×10^{-2}	26.99×10^{-2}
Efficiency	Time/h	0.97	4.98	5.29	60.50
	Ratio	1.0	5.13	5.45	62.4

The steel specifications used on each floor are provided in Table 4. By comparing with the alternative methods, it can be found that the proposed method meets both accuracy and efficiency requirements. In the optimization result, the minimum steel consumption of the structure that can meet the probability constraint is $26.99\times10^{-2}m^3$.

4.4 Example 4: Topology optimization of twelve-story braced composite steel frame

The fourth example focuses on a twelve-story planar braced composite steel frame, as illustrated in Fig. 9. Each floor of the structure has a mass of 25×10^4kg, with a floor height of 4.2 meters and a bay width of 6.0 meters. The stiffness of the beams is assumed to be infinite. The columns are constructed by HM594×302×14×23 specification steel materials, with an elastic modulus of E=210GPa and a section moment of inertia of $I_x=137000cm^4$. The structure incorporates diagonally-crossed rods as braces, providing a lateral stiffness of $k=0.67\times10^8$N/m. Considering a damping ratio of $\zeta=5\%$, the structure is subject to the same excitation model as in Example 3, except with $S_0=200.177\times10^{-4}m^2/s^3$ for rare earthquakes. Failure occurs if the top displacement of the structure exceeds 0.8m, considering a total of $m=50000$ sample groups. Two types of reliability design optimization problems are conducted for the structure.

Optimization problem 1: The objective is to minimize the number of braces while ensuring that the reliability index of the structure is not less than 3.20, and provide the best layout plan.

Optimization problem 2: The objective is to calculate the maximum reliability index of the structure while keeping the number of braces arranged below 40, and provide the best layout plan.

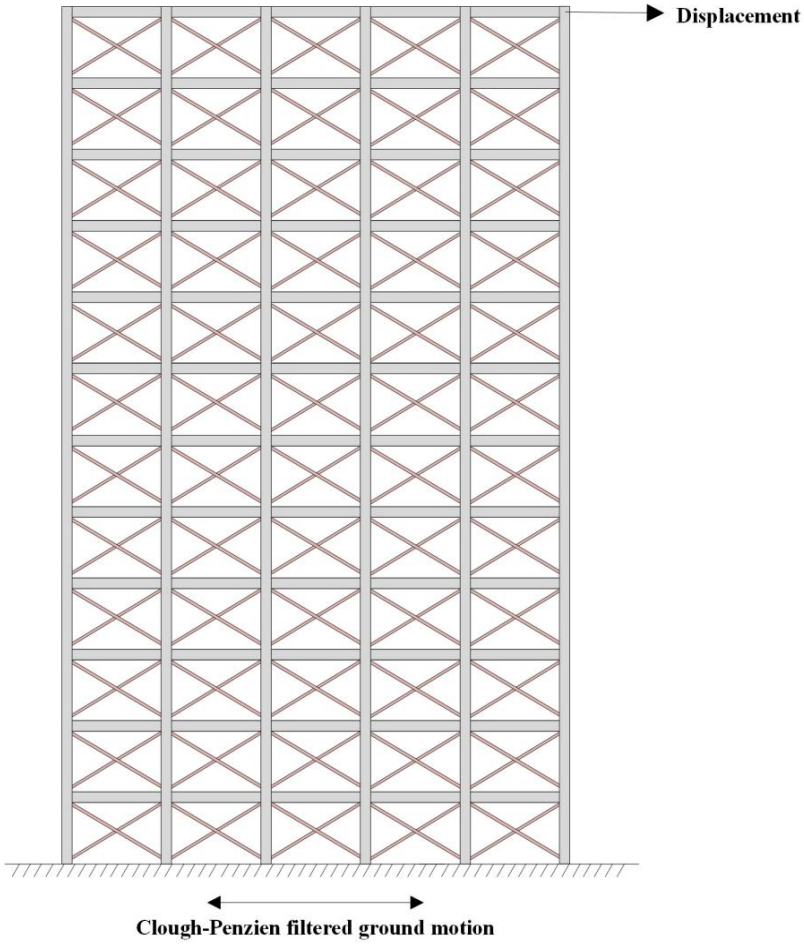

Fig. 9 Model of a 12-story braced composite steel frame

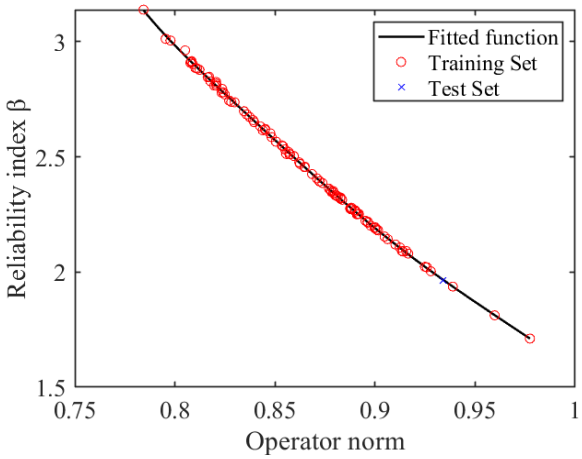

Fig. 10 Operator norm-reliability index mapping function for Example 4

$$\varphi(\beta) = -0.02\beta^6 + 0.39\beta^5 - 2.57\beta^4 + 8.79\beta^3 - 16.52\beta^2 + 16.02\beta - 5.20 \tag{38}$$

Fig. 10 presents a mapping function for Example 4 with 100 sample points. Based on Eq(35), the original optimization problems are transformed. Optimization problem 1 can be expressed as follows:

$$\min \sum_{i=1}^{12} N_i$$

subject to:

$$\beta \geq 3.20 \Rightarrow \| \mathrm{A(y)} \|_{\infty,2} \leq \varphi(3.20) \tag{39a}$$

$$N_i \in [0,1,2,3,4,5]$$

$$\max \beta \Rightarrow \min \| \mathrm{A(y)} \|_{\infty,2}$$

subject to:

$$\sum_{i=1}^{12} N_i \leq 40 \tag{39b}$$

$$N_i \in [0,1,2,3,4,5]$$

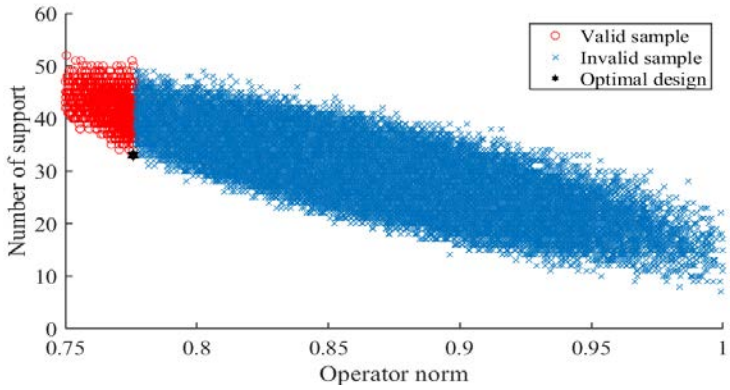

Fig. 11 Scatter plot of sample operator norm-brace quantity for Problem 1

Table 5 Optimization results for Problem 1 of Example 4

Method	Floor	Brace No.	Floor	Brace No.	Floor	Brace No.	Total No.	β	Efficiency	
									Time/h	Ratio
Proposed method	1st	5	5th	3	9th	1	32	3.21	1.47	1.0
	2nd	5	6th	3	10th	1				
	3rd	4	7th	2	11th	1				
	4th	4	8th	2	12th	1				
AK-MCS	1st	4	5th	5	9th	0	33	3.21	10.54	7.17
	2nd	4	6th	5	10th	0				
	3rd	5	7th	5	11th	0				
	4th	3	8th	1	12th	1				
Response surface	1st	5	5th	3	9th	1	33	3.20	11.36	7.73
	2nd	4	6th	3	10th	0				
	3rd	5	7th	4	11th	0				
	4th	4	8th	4	12th	0				
Monte Carlo	1st	5	5th	4	9th	0	33	3.23	152.39	103.7
	2nd	4	6th	3	10th	1				
	3rd	5	7th	5	11th	1				
	4th	4	8th	1	12th	0				

With Eq(35), Optimization Problem 2 can be transformed into:

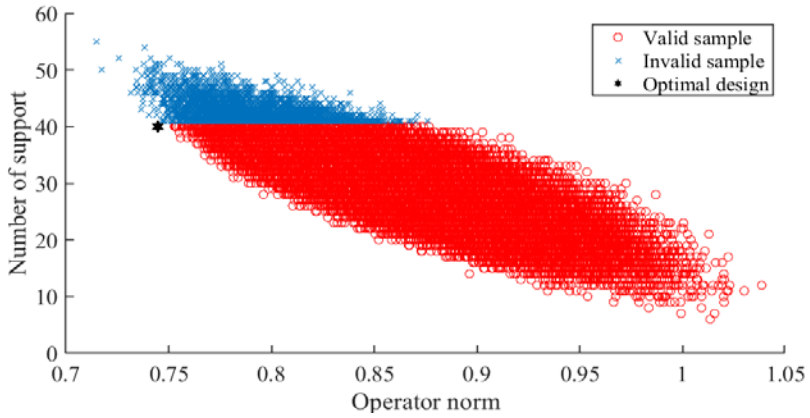

Fig. 12 Scatter plot of sample operator norm-brace quantity for Problem 2

Table 6 Optimization results for Problem 2 of Example 4

Method	Floor	Brace No.	Floor	Braces No.	Floor	Brace No.	Total No.	β	Efficiency	
									Time/h	Ratio
Proposed method	1st	5	5th	5	9th	2	40	3.54	1.42	1.0
	2nd	5	6th	5	10th	0				
	3rd	5	7th	4	11th	2				
	4th	5	8th	2	12th	0				
AK-MCS	1st	5	5th	5	9th	3	40	3.46	9.92	6.99
	2nd	4	6th	2	10th	0				
	3rd	5	7th	5	11th	3				
	4th	5	8th	3	12th	0				
Response surface	1st	4	5th	5	9th	2	40	3.41	10.13	7.13
	2nd	5	6th	4	10th	2				
	3rd	5	7th	4	11th	0				
	4th	5	8th	3	12th	1				
Monte Carlo	1st	5	5th	3	9th	0	40	3.46	150.87	106.2
	2nd	5	6th	5	10th	0				
	3rd	5	7th	4	11th	3				
	4th	5	8th	4	12th	1				

The calculation and analysis of the structural dynamic response operator norm for the extracted samples are based on the transformed optimization problems. The distribution maps of the operator norm-bracing quantity for the 50000 sample groups are presented in Figs. 11 and 12. In these sample points, the red region represents

valid samples, while the blue region represents invalid samples. The optimal design points are identified by finding the minimum number of brace layouts and the minimum operator norm value from the valid samples. These optimal design points are depicted as black solid hexagonal in Figs. 11 and 12.

The analysis findings demonstrate that in order to satisfy the reliability index is not less than 3.20, a minimum of 32 braces must be installed in the structure. Furthermore, it is possible to achieve the highest reliability index of 3.54 while ensuring that the number of braces does not exceed 40.. After comparison, it is evident that the proposed method exhibits significant efficiency advantages, and achieved better design schemes. The optimal layout schemes for braces in the two optimization problems are provided in Tables 5 and 6 respectively, while the specific layout scheme is illustrated in Fig. 13. The analysis demonstrates that placing a larger number of brace rods at the bottom of the structure and gradually transitioning upwards can enhance the reliability performance and improve the rationality of the design.

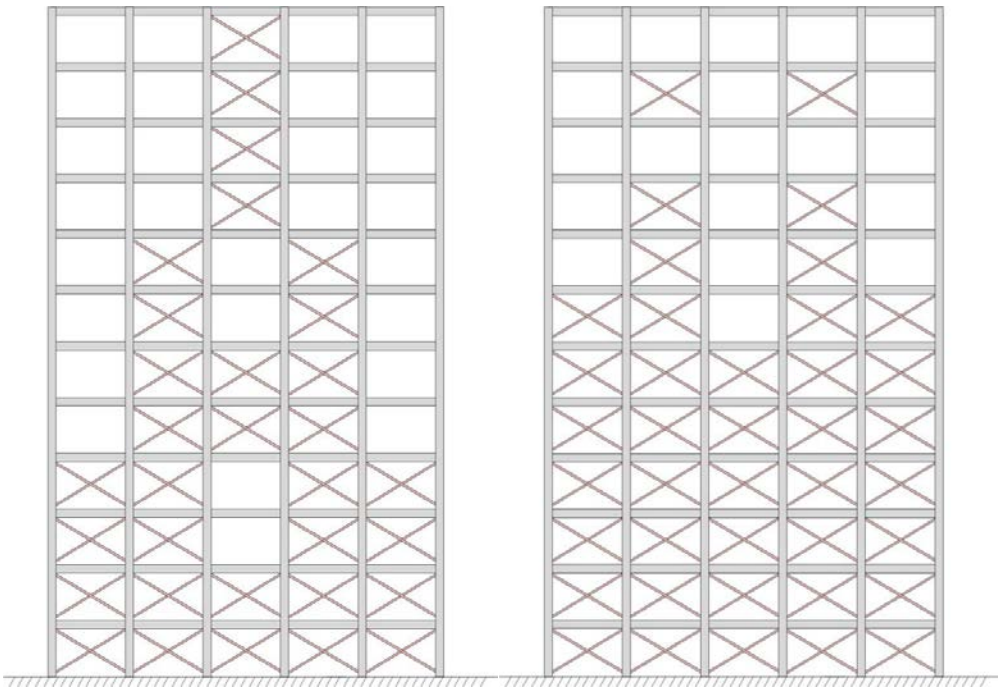

(a)Optimization result 1 (b)Optimization result 2

Fig. 13 Optimization layout scheme for Example 3

5. Conclusion

This study proposes an efficient method based on mapping between reliability and operator norm for dynamic reliability-based design optimization. With the

mapping, the probability constraints can be transformed into deterministic constraints in reliability optimization problems, effectively improving the efficiency of RBDO under random excitation. The accuracy and applicability of the proposed method are verified through numerical examples, leading to the following key findings:

(1) Based on the K-L expansion of random excitations, the mapping relationship between first excursion reliability and operator norm can be effectively established within the the operator norm framework.

(2) The established mapping function enables the transformation of complex reliability design optimization problems into deterministic optimization problems, eliminating the need for reliability analysis in the optimization process while preserving the original optimization objectives. Compared to conventional RBDO methods, the proposed method demonstrates higher accuracy and efficiency. In certain scenarios, the optimization efficiency can be improved by over 100 times.

(3) The proposed method proves to be effective in addressing reliability-constrained or cost-constrained optimization problems and demonstrates wide applicability in various optimization scenarios, including parameter optimization, cost optimization, and topology optimization.

Acknowledgment

The research is supported by the National Natural Science Foundation of China (Grant No.52378126), and the Provincial Natural Science Foundation of Hunan, China (Grant Nos.2022JJ10050 and 2023JJ40036). The support is gratefully acknowledged.

References

[1] Taflanidis A A, Scruggs J T. Performance measures and optimal design of linear structural systems under stochastic stationary excitation. Structural Safety. 2010;32(5): 305-315. https://doi.org/10.1016/j.strusafe.2010.03.010.

[2] Zheng XW, Li HN, Gardoni P. Reliability-based design approach for high-rise buildings subject to earthquakes and strong winds. Engineering structures. 2021;244:112771. https://doi.org/10.1016/j.engstruct.2021.112771.

[3] Jiang YB, Li ZM, Zhou H, et al. Reliability evaluation of RC columns with wind-dominated combination considering random biaxial eccentricity. Journal of

Structural Engineering. 2022;149(1): 06022007,1-06022007,6. https://doi.org/10.1061/(ASCE)ST.1943-541X.0003507.
[4] Schuëller G I, Jensen H A. Computational methods in optimization considering uncertainties - an overview. Computer Methods in Applied Mechanics and Engineering. 2008;198(1): 2-13. https://doi.org/10.1016/j.cma.2008.05.004.
[5] Taflanidis A A. Reliability-based optimal design of linear dynamical systems under stochastic stationary excitation and model uncertainty. Engineering Structures. 2010;32(5):1446-1458. https://doi.org/10.1016/j.engstruct.2010.01.023.
[6] Yang M, Zhang D, Han X. New efficient and robust method for structural reliability analysis and its application in reliability-based design optimization. Computer Methods in Applied Mechanics and Engineering. 2020;366:113018. https://doi.org/10.1016/j.cma.2020.113018.
[7] Yang M, Zhang D, Jiang C, et al. A hybrid adaptive Kriging-based single loop approach for complex reliability-based design optimization problems. Reliability Engineering & System Safety. 2021;215:107736.https://doi.org/10.1016/j.ress.2021. 107736.
[8] Wang Y, Hao P, Yang H, et al. A confidence-based reliability optimization with single loop strategy and second-order reliability method. Computer Methods in Applied Mechanics and Engineering. 2022;372:113436.https://doi.org/10.1016/j.cma. 2020.113436.
[9] Liu X, Li TR, Zhou ZH, et al. An efficient multi-objective reliability-based design optimization method for structure based on probability and interval hybrid model. Computer Methods in Applied Mechanics and Engineering. 2022;296:115862.https://doi.org/10.1016/j.cma.2022.114682.
[10] Yang M, Zhang D, Wang F, et al. Efficient local adaptive Kriging approximation method with single-loop strategy for reliability-based design optimization. Computer Methods in Applied Mechanics and Engineering. 2022;390:114462.https://doi.org/10.1016/j.cma.2021.114462.
[11] Jiang YB, Zhao LJ, Beer M, et al. Multiple response surfaces method with advanced classification of samples for structural failure function fitting. Structural Safety. 2017;64:87-97.https://doi.org/10.1016/j.strusafe.2016.10.002.
[12] Jensen H A, Jerez D J, Valdebenito M. An adaptive scheme for reliability-based global design optimization: A Markov chain Monte Carlo approach. Mechanical Systems and Signal Processing. 2020;143: 106836. https://doi.org/10.1016/j.ymssp.2020.106836.
[13] Yuan XK, Valdebenito M A, Zhang BQ, et al. Efficient decoupling approach for reliability-based optimization based on augmented Line Sampling and combination algorithm. Computers & Structures. 2023;280:107003.https://doi.org/ 10.1016/j.compstruc.2023.107003.
[14] Ali K, Ataollah Z. Reliability-based design optimization of the frame structures using the force method and SORA-DM framework. Structures.

2022;45:814-827.https://doi.org/10.1016/j.istruc.2022.09.057.
[15]Faes M, Valdebenito M. Fully decoupled reliability-based optimization of linear structures subject to gaussian dynamic loading considering discrete design variables. Mechanical Systems and Signal Processing. 2021;159:107616. https://doi.org/10.1016/j.ymssp.2021.107616.
[16]Zou T, Mahadevan S. A direct decoupling approach for efficient reliability-based design optimization. Structural and Multidisciplinary Optimization. 2006;31: 190-200. https://doi.org/10.1007/s00158-005-0572-7.
[17]Li J, Chen J B. Probability density evolution method for dynamic response analysis of structures with uncertain parameters. Computational Mechanics. 2004;34:400-409. https://doi.org/10.1007/s00466-004-0583-8.
[18]Yang JS, Chen JB, Jensen H. Structural design optimization under dynamic reliability constraints based on the probability density evolution method and highly-efficient sensitivity analysis. Probabilistic engineering mechanics. 2022;68:103205. https://doi.org/10.1016/j.probengmech.2022.103205.
[19]Au S K, Beck J L. First excursion probabilities for linear systems by very efficient importance sampling. Probabilistic Engineering Mechanics. 2001;16(3):193-207. https://doi.org/10.1016/S0266-8920(01)00002-9.
[20]Au S K, Beck J L. Subset Simulation and its Application to Seismic Risk Based on Dynamic Analysis. Journal of Engineering Mechanics. 2003;129(8):901-917. https://doi.org/10.1061/(ASCE)0733-9399(2003)129:8(901).
[21]Ankur S, Tharo S, Kalyanmoy D. Using Karush-Kuhn-Tucker proximity measure for solving bilevel optimization problems. Swarm and Evolutionary computation. 2019;44:496-510.https://doi.org/10.1016/j.swevo.2018.06.004.
[22]Dubourg V, Sudret B, Bourinet J M. Reliability-based design optimization using kriging surrogates and subset simulation. Structural and Multidisciplinary Optimization. 2011;44: 673-690. https://doi.org/10.1007/s00158-011-0653-8.
[23]Sudret B. Global sensitivity analysis using polynomial chaos expansions. Reliability engineering & system safety. 2008;93(7): 964-979. https://doi.org/10.1016/j.ress.2007.04.002.
[24]Mohammad AF, Seyed RHV. A decoupled double-loop method with the adaptive allowable limits for probabilistic performance-based design optimization. Engineering Structures. 2023;279:115634.https://doi.org/10.1016/j.engstruct.2023.115634.
[25]Yuan XK, Liu SL, Valdebenito M A, et al. Decoupled reliability-based optimization using Markov chain Monte Carlo in augmented space. Advances in Engineering Software. 2021;157-158:103020.https://doi.org/10.1016/j.advengsoft.2021.103020.
[26]Zhao Z, Zhao YG , Li PP. A novel decoupled time-variant reliability-based design optimization approach by improved extreme value moment method. Reliability Engineering and System Safety. 2023;229:108825.https://doi.org/10.1016/j.ress.2022.108825.

[27] Faes M, Valdebenito M A. Fully decoupled reliability-based design optimization of structural systems subject to uncertain loads. Computer Methods in Applied Mechanics and Engineering. 2020;371:113313.https://doi.org/10.1016/j.cma.2020.113313.
[28] Ni P, Jerez D J, Fragkoulis V C, et al. Operator norm-based statistical linearization to bound the first excursion probability of nonlinear structures subjected to imprecise stochastic loading. ASCE-ASME Journal of Risk and Uncertainty in Engineering Systems, Part A: Civil Engineering. 2022;8(1): 04021086. https://doi.org/10.1061/AJRUA6.0001217.
[29] Faes M, Valdebenito M A, Moens D, et al. Operator norm theory as an efficient tool to propagate hybrid uncertainties and calculate imprecise probabilities. Mechanical Systems and Signal Processing. 2020;152:107482. https://doi.org/10.1016/j.ymssp.2020.107482.
[30] Jerez D J, Jensen H A, Beer M. Reliability-based design optimization of structural systems under stochastic excitation: an overview. Mechanical Systems and Signal Processing. 2022;166: 108397. https://doi.org/10.1016/j.ymssp.2021.108397.
[31] Valdebenito M A, Jensen H, Labarca AA. Estimation of first excursion probabilities for uncertain stochastic linear systems subject to Gaussian load. Computers & Structures. 2014;138:36-48.https://doi.org/10.1016/j.compstruc.2014.02.010.
[32] Stefanou G. The stochastic finite element method: past, present and future. Computer methods in applied mechanics and engineering. 2009;198(9-12): 1031-1051. https://doi.org/10.1016/j.cma.2008.11.007.
[33] B. Echard, N. Gayton, M. Lemaire. AK-MCS: An active learning reliability method combining Kriging and Monte Carlo Simulation. Structural Safety. 2011;33(2):145-154.https://doi.org/10.1016/j.strusafe.2011.01.002.
[34] Gao S Z, Zhao Y K, Zhao X D, et al. Application of response surface method based on new strategy in structural reliability analysis. Structures. 2023;57:105202. https://doi.org/10.1016/j.istruc.2023.105202.
[35] Zerva A. Spatial variation of seismic ground motions: modeling and engineering applications. 2016.
[36] M. Amin, A.H.S. Ang. Non-stationary stochastic model of earthquake motion. Journal of Engineering Mechanics Dicision, ASCE. 1968;94(EM2):559~583. https://doi.org/10.1061/JMCEA3.0000969.

Appendix

Appendix Table 1 HM Steel Specification Table

HM Steel Specification $h\times b\times t_1\times t_2$(mm)	Cross-sectional area A(cm^2)	Mass m(kg/m)	Moment of inertia I_x(cm^4)
148×100×6×9	27.25	21.4	1040
194×150×6×9	39.76	31.2	2740
244×175×7×11	56.24	44.1	6120
294×200×8×12	73.03	57.3	11400
340×250×9×14	101.5	79.7	21700
390×200×10×16	136.7	107	38900
440×300×11×18	157.4	124	56100
482×300×11×15	146.4	115	60800
488×300×11×18	164.4	129	71400
582×300×12×17	174.5	137	103000
588×300×12×20	192.5	151	118000
594×302×14×23	222.4	175	137000